ACS APPLIED MATERIALS & INTERFACES

Research Article

www.acsami.org

Mesoporous Nanostructured Nb-Doped Titanium Dioxide Microsphere Catalyst Supports for PEM Fuel Cell Electrodes

Laure Chevallier,[†] Alexander Bauer,[‡] Sara Cavaliere,[†] Rob Hui,[‡] Jacques Rozière,[†] and Deborah J. Jones*[,†]

[†]Institut Charles Gerhardt, Agrégats, Interfaces et Matériaux pour l'Energie, UMR CNRS 5253, Université Montpellier II, 34095 Montpellier Cedex 5, France

[‡]Institute for Fuel Cell Innovation, National Research Council of Canada, 4250 Wesbrook Mall, Vancouver, B.C., Canada V6T 1W5

ABSTRACT: Crystalline microspheres of Nb-doped TiO_2 with a high specific surface area were synthesized using a templating method exploiting ionic interactions between nascent inorganic components and an ionomer template. The microspheres exhibit a porosity gradient, with a meso-macroporous kernel, and a mesoporous shell. The material has been investigated as cathode electrocatalyst support for polymer electrolyte membrane (PEM) fuel cells. A uniform dispersion of Pt particles on the Nb-doped TiO_2 support was obtained using a microwave method, and the electrochemical properties assessed by cyclic voltammetry. Nb-TiO_2 supported Pt demonstrated very high stability, as after 1000 voltammetric cycles, 85% of the electroactive Pt area remained compared to 47% in the case of commercial Pt on carbon. For the oxygen reduction reaction (ORR), which takes place at the cathode, the highest stability was again obtained with the Nb-doped titania-based material even though the mass activity calculated at 0.9 V vs RHE was slightly lower. The microspherical structured and mesoporous Nb-doped TiO_2 is an alternative support to carbon for PEM fuel cells.

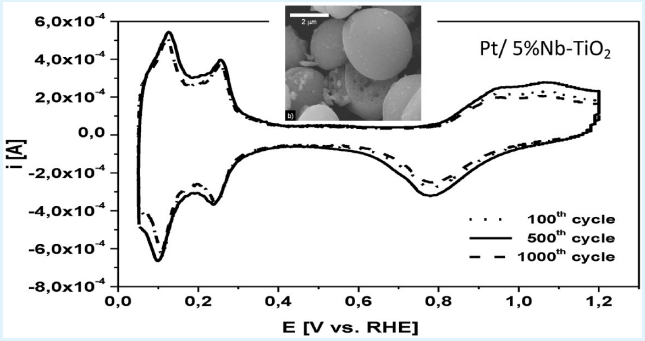

KEYWORDS: *doped titania, PEMFC, electrocatalyst, mesoporous materials, microspheres*

INTRODUCTION

High-temperature PEM fuel cells operating at temperatures higher than 80 °C are the next generation of fuel cell technology. By operating at such a temperature the reaction kinetics, the catalyst tolerance toward contaminants, the heat rejection, and the water management are significantly improved.[1−4] One of the challenges in the development of high-temperature PEM fuel cells is the improvement of the catalyst support properties.[5] In the first instance, some studies introduced novel nanostructured carbon supports as discussed by Antolini[6] and Shao,[7] who demonstrated that a significant mesoporosity influences the electrochemical performance of PEM fuel cells. If compared to conventional Vulcan XC-72 carbon black, nanostructured mesoporous carbon enhances the three phase boundary, allows a high and uniform dispersion of Pt, and enhances the electron transfer because of the specific pore structure.[6,7]

Another crucial issue, which has yet to be overcome to increase the lifetime of the cell, is carbon support degradation caused by carbon corrosion or oxidation.[8,9] Carbon oxidation leads to a loss of noble metal catalyst from the support surface, Pt migration and agglomeration of Pt particles, and a reduction of the electroactive catalyst surface area. Alternative materials to replace carbon have been studied, such as electronically conductive ceramics,[7,10,11] and it was demonstrated that using metal oxides as catalyst supports could significantly increase the stability of the cell, and furthermore reduce the cost of the PEMFC, by decreasing the platinum loading.[12,13] Metal oxides could also play the role of a cocatalyst by promoting the catalytic performance as a result of a strong metal−support interaction.[14] Novel catalyst supports must be electronically conductive and have a high specific surface area and a suitable porosity, and allow a high dispersion of the platinum nanocatalyst. It has been shown recently that a TiO_2-based cermet could be a good candidate as a catalyst support.[15,16] However, pure titanium oxide is electrically insulating at temperatures below 200 °C and to induce electronic conductivity, further modifications are necessary. Preparing substoichiometric titania based materials improved the electronic conductivity[17] but the stability of the support after extensive polarization at positive potentials has to be validated.[18,19] Another approach is to dope titania with an *n*-type dopant such as niobium.[20−25] Depending on the atmosphere and the temperature used during calcination, TiO_2 is present as anatase or rutile, and the electronic conductivity is improved.[22,26]

Combining good electrocatalytic properties and electronic conductivity within a nanostructure with controlled porosity

Received: January 1, 2012
Accepted: March 5, 2012
Published: March 19, 2012

   dx.doi.org/10.1021/am300002j | *ACS Appl. Mater. Interfaces* 2012, 4, 1752−1759

would lead to a very appealing catalyst support. The Pt dispersion and its effective loading would be better controlled and the porosity would boost the catalytic performance because of better gas permeation. Mesoporous TiO_2 with/without a specific nanostructure has been widely investigated following a variety of synthesis procedures using templates such as alkyl phosphate anionic surfactants,[27] quaternary ammonium cationic templates,[28−30] primary amines,[31,32] amphiphilic block copolymers,[33] or nonsurfactant templates.[34,35] Recently conducted research also discussed free-template synthesis processing.[36] However, only for a few materials are the surface area, pore structure, and morphology stable at the higher temperatures leading to the more crystalline electronic conducting phases relevant for PEMFC application. Other porous TiO_2 structures can also be prepared, such as nanotubes, nanofibers or nanorods.[37−40] To the best of our knowledge, little research has focused on using these different types of morphologies for PEM electrodes applications.[39,41−47]

In this work, an innovative and simple synthesis of Nb-doped mesoporous nanocrystalline TiO_2 microspheres is proposed. It makes use of ionic interactions between nascent inorganic components and an ionomer in solution in a high dielectric constant solvent in an approach derived from the work of Chujo et al.,[48] who used sulfonated polystyrene to obtain nanometer scale homogeneous polystyrene and SiO_2 polymer hybrids. It is known that polyelectrolytes of sufficiently high acidic characteristics, such as acid-functionalized ionomers, have a distinct morphology arising from self-organization, which is related to that shown by amphiphilic systems.[49] An ionomer belonging to the polyetherketone family (sulfonated poly(ether ether ketone) sPEEK) was used as a reaction and templating medium with a TiO_2 precursor. sPEEK was chosen because its degree of sulfonation (DS) can be easily controlled.[50] This allows the facile tuning of the ionic polyelectrolyte/TiO_2 precursor interactions and consequently the control of the final material morphology and porosity. After calcination of the polymer hybrid sPEEK-TiO_2 precursor at 500 °C, a nanostructured niobium-doped (5 and 10 at % Nb-doped) TiO_2 anatase is obtained with a specific surface area up to 150 $m^2\ g^{-1}$. The material is then used as a catalyst support for ORR, and the Pt catalyst is deposited by a microwave driven impregnation process. The mesoporous microspheres supported catalyst shows encouragingly stable electrochemical properties on voltage cycling, compared to the commercially available carbon supported catalyst, and thus becomes a promising candidate as catalyst support for high-temperature PEM fuel cells.

EXPERIMENTAL SECTION

Materials. Poly(ether ether ketone) (PEEK), Victrex 450-P with a molecular weight of 1×10^5 g·mol^{-1} and particle size of 80 μm was obtained from Goodfellow. Dimethylsulfoxide (DMSO), sodium hydroxide (NaOH), absolute ethanol, isopropanol, titanium(IV) oxysulfate sulfuric acid complex hydrate, ammonium niobate oxalate hydrate and $H_2PtCl_6{\cdot}xH_2O$ were purchased from Sigma-Aldrich. E-Tek carbon and the Nafion solution (5 wt % in a mixture of water and alcohol) were purchases from Alfa Aesar.

Synthesis of Nb-Doped TiO_2 Microspheres. Sulfonation of PEEK was carried out as described elsewhere.[50] A range of sPEEK samples were synthesized by varying the degree of sulfonation (DS) between 50 and 75%, and the influence of DS on the resulting structure of TiO_2 was investigated. By varying the DS, spherical, ellipsoidal or unstructured titania based materials were obtained. An sPEEK ionomer with a DS of 60% led to a high dispersion of regular spheres, and this formulation was applied for the remainder of the study.

Typically, 1 g of the sulfonated polymer was dissolved in DMSO in 10 wt % concentration at 110 °C under vigorous stirring. A clear solution was obtained. A solution of 1.15 g of titanium oxysulfate hydrate in a minimum amount of DMSO was prepared. Nb-doped TiO_2 was obtained by adding an appropriate amount of niobate salts to the solution of titanium oxysulfate. Since the literature[23,24,51] shows that the solubility limit of Nb into anatase is around 10 $_{at.}$%, two concentrations for Nb doping were investigated, namely 5 and 10 at %. The salts solution was added dropwise to the polymer solution in such a way that the weight fraction of TiO_2 (calculated from the titanium content) loaded in the polymer solution was 25 wt %. The solution was stirred at 110 °C for 2 h, until a clear solution was obtained again, indicating the complete dissolution of the salts in the ionomer solution. The solution was poured into a Petri dish and dried overnight, yielding an opaque membrane. Nb doped-TiO_2 microspheres were obtained after calcination at 500 °C for 2 h. These powders were submitted to ultrasound treatment for 2 h in ethanol, washed with distilled water and dried at 80 °C overnight.

Synthesis of Nb-Doped−TiO_2-Supported Platinum. Platinum deposition on the Nb-TiO_2 supports was carried out using a microwave assisted method.[52] A deposition bath was prepared by mixing 50 mg of mesoporous Nb-doped TiO_2 microspheres in 50 mL of ethylene glycol and the desired amount of the catalyst precursor H_2PtCl_6. The slurry was stirred vigorously for 20 min. The pH was adjusted to 9 with a 1 M NaOH containing ethylene glycol solution. The bath was placed in a microwave oven and heated at a setting of 600 W for 60 s. In total the 60 s microwaving interval was carried out four times and between each microwave interval, the slurry was stirred at room temperature for 5 min. The solvent was removed by centrifugation, which was carried out four times for 10 min at 11 000 rpm, while replacing the liquid with fresh deionized H_2O each time. The Pt/Nb-TiO_2 catalyst was dried in an oven at 80 °C overnight.

Materials Characterization. Microstructural and morphological characterizations were carried out on both undoped and Nb-doped TiO_2, and on Pt catalyst coated powders by using X-ray diffraction (XRD), scanning electron microscopy (SEM), transmission electron microscopy (TEM), nitrogen adsorption/desorption, and X-ray photoelectron spectroscopy (XPS). Crystallographic characteristics of the materials were investigated by XRD using a Philips X'Pert diffractometer (Cu Kα_1 radiation) in a Bragg−Brentano configuration at a scanning rate of 0.0015° per second with 2θ ranging from 20 to 85°. The morphology of the powders was observed by SEM imaging using a JEOL scanning electron microscope (JSM-6300F) and by TEM imaging using a JEOL 1200 EXII microscope operating at 120 kV. Due to the diameter and thus the thickness of the microspheres, cross-sectional samples were prepared for the TEM analysis. The samples were embedded in an epoxy resin and dried at 80 °C for 24 h. Microtomed sections of 70 to 90 nm thickness were prepared using a Reichert ultramicrotome and deposited on copper grids (Agar). The BET specific surface area (S_{BET}) was determined from N_2 gas adsorption−desorption measurements at −196 °C using an automated volumetric apparatus (Micromeritics ASAP 2020 MP) assuming a surface area of 0.162 nm^2 per nitrogen molecule.[53] By using the Barret-Joyner-Halenda (BJH) model, the pore volumes and pore size distributions were derived from the desorption branches of isotherms. Prior to the adsorption measurements, all samples were heat treated at 80 °C under vacuum (1×10^{-5} Torr) for 10 h. The surface composition of the catalysts was monitored by XPS on an ESCALAB 250 (Thermo Electron). The X-ray excitation was provided by a monochromatic Al K_α (1486.6 eV) source. The analyzed surface area was 400 μm^2. The detection of the emitted photoelectrons was performed in a direction that was perpendicular to the surface sample. Data analysis was performed using the Avantage software. The background signal was removed using the Shirley method,[54] and the surface atomic concentrations were determined from photoelectron peak areas using the atomic sensitivity factors reported by Scofield.[55] Binding energies (BE) of all core levels were referred to the C−C bond of C 1s at 284.8 eV.

Electrochemical Characterization. The electrical conductivities of the titania microspheres were measured at room temperature using an in-house conductivity cell using the conventional four-probe method and Van Der Pauw calculations[31]. Catalyst supports were mixed with Nafion ionomer dispersion in isopropanol (20% in volume) purchased from Aldrich used as binder and pressed into pellets at 880 MPa. The electrochemical experiments were carried out using a three-electrode glass cell and a Solartron multistat instrument (controlled with Corrware software, Scribner Associates Inc., USA). The counter electrode was a Pt wire, a $Hg/HgSO_4$ type electrode containing a 30 wt % sulfuric acid solution (Koslow Scientific) was used as the reference electrode, and the working electrode was a glassy carbon rotating disk electrode (RDE) with a geometric area of 0.196 cm^2 from Pine Instrument. The catalyst ink was prepared by dispersing the catalyst powder in isopropanol (2.4 mg mL^{-1}) by ultrasonication for 20 min. It was then deposited onto the RDE surface with a micropipette. Knowing the platinum loading on the titania supports to be 20 wt %, and the exact volume deposited on the glassy carbon electrode, a Pt loading per geometric area of 48 $\mu g\ cm^{-2}$ was calculated. After drying, 7.1 μL of 0.05 wt % Nafion in methanol solution was added to the catalyst powder-coated RDE. All electrochemical tests were carried out at 20 °C and ambient pressure and all potential values are reported with respect to the reversible hydrogen electrode (RHE).

Each freshly prepared electrode was cycled 20 times in N_2 purged 0.5 M H_2SO_4 in the potential range from 0.05 to 1.2 V vs RHE at a scan rate of 50 mV s^{-1} to clean the Pt surface. Cyclic voltammetry was then carried out at 100 mV s^{-1}, performing 1000 full cycles from 0.05 to 1.2 V vs RHE. To evaluate the stability of the catalyst support, the decrease of the active Pt surface area was calculated from the voltammograms after 100, 500, and 1000 cycles, based on H_2 desorption peaks in the range from 0.05 to 0.35 V vs RHE and assuming a hydrogen desorption charge of 210 $\mu C\ cm^{-2}$ for the electroactive Pt surface.[56] The oxygen reduction reaction (ORR) experiment was performed on 20 wt %Pt/Nb-doped TiO_2 and on reference E-TEK electrodes using linear sweep voltammetry at a rotation rate of 900 rpm with O_2 saturated 0.5 M H_2SO_4, both on the Pt on The potential was decreased from 1.1 to 0.2 V vs RHE at a scan rate of 5 mV s^{-1}. To investigate the electrochemical durability of the samples, an accelerated stability test was performed, and the final ORR activity was recorded.[43,57] The ORR activity was determined for "fresh" catalysts, and for "aged" catalysts subjected to 1000 voltammetric cycles as described above.

RESULTS AND DISCUSSION

Nb-Doped TiO_2 Characterization. The XRD measurements obtained for both undoped and doped TiO_2 after air calcination at 500 °C are shown in panels a and b in Figure 1, respectively. The anatase phase (JCPDS 21−1272) was observed in both cases. The absence of Nb_2O_5 phase in the Nb-doped TiO_2 indicates that doping was effective.

Figure 2a shows the SEM micrographs of the polymer hybrid membrane, whereas Figure 2b−d shows the 5 at % Nb-doped TiO_2 powders obtained after calcination at 500 °C. Secondary electron measurements are presented in images b and d in Figure 2, whereas backscattered imaging is shown in images a and c. A high dispersion of regular microspheres embedded in the ionomer template is clearly observed in Figure 2a. The estimated diameter of the spheres was in the 2−4 μm range. Figure 2b shows the microspheres obtained after calcination at 500 °C, with a diameter confirmed between 2 and 4 μm. A rough surface can be clearly observed with an internal macroporosity, giving rise to a spongelike structure. In Figure 2c, a multilength scale porosity is observed from the back scattered imaging. Figure 2d shows a gradient of porosity from an internal macroporous core having interconnected porosity to a denser outer shell. Figure 3a shows the TEM micrograph of a

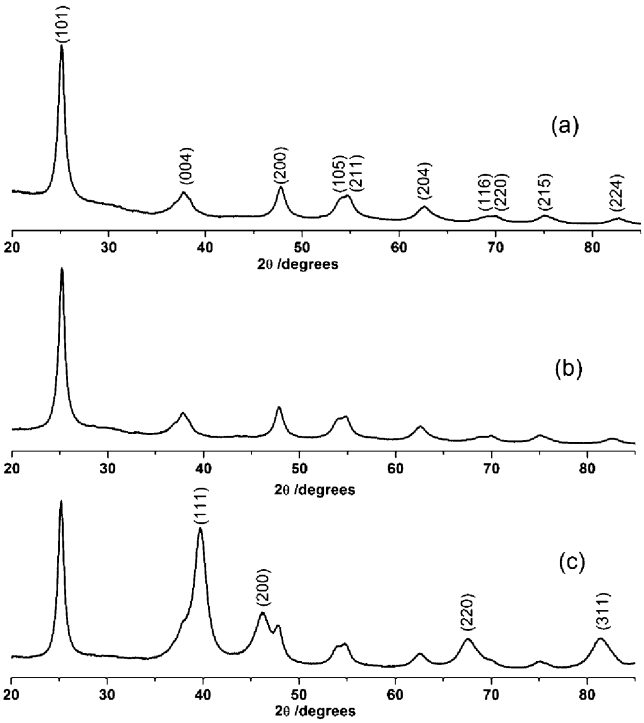

Figure 1. XRD patterns of (a) undoped TiO_2 microspheres, (b) 5 at % Nb-doped TiO_2, and (c) 20 wt % Pt/5 at % Nb-doped TiO_2 materials. The Miller indices in graph a identified the anatase TiO_2 phase, whereas the ones in c identified Pt^0 phase.

microtomed section of the 5 at % Nb-doped TiO_2 microspheres. The core comprises agglomerated Nb-doped titania particles with an average grain size of 9 nm, while the outer shell part is formed of smaller Nb-doped TiO_2 nanoparticles with a wormhole-like mesoporosity. Corroborating XRD, TEM and SEM results were obtained for 10 at % Nb-doped TiO_2 powders (not shown here) signifying no or only a slight influence of the doping on the titanium-based materials' morphology. The final structure probably evolves through several complex processes. At the largest macroscopic level, local phase inversion in solvent-rich and solvent-poor regions involving water produced by hydrolysis of the titania precursor, leads to a spherical morphology. At the nano/mesoscopic scale, the influence of the nanophase separation and the clustering of the ionogenic groups around the solvent phase in the ionomer is involved, leading to the mesoporous texture observed for the final material.[48] Thus, depending on experimental parameters (DS, reactant concentration in DMSO), the titania precursor salts selectively assemble within the ionic regions of the ionomer. Water formed during hydrolytic polycondensation of titania causes local phase inversion and precipitation of sPEEK within a hybrid titania-sPEEK mesostructure. Mesoporous titania is formed upon thermal removal of the organic matrix porogen.

The nitrogen adsorption/desorption isotherms of the 5 at % Nb-doped TiO_2 powder in Figure 4 provide evidence for the presence of two kinds of pores. A distinct hysteresis loop is observed in the range P/P_o equal to 0.4−0.8, indicating the presence of a large fraction of mesopores. Furthermore, a smaller hysteresis loop is present in the 0.8−1 range, indicating some interparticle porosity. The parallel shape of the curves in the capillary condensation region suggests uniform tubular pores, while the distribution of pores shown in the inset

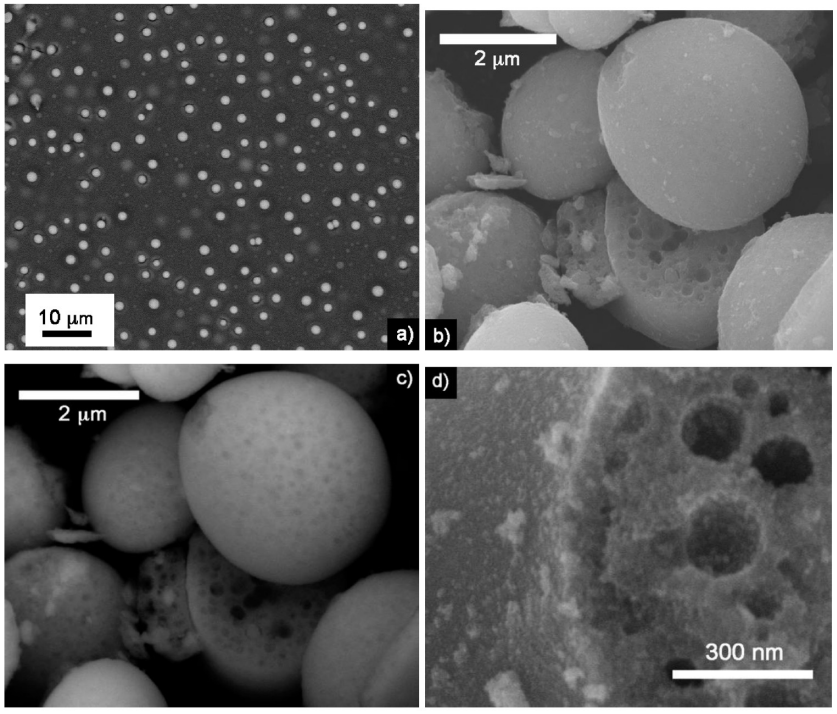

Figure 2. SEM micrographs of (a) the hybrid membrane and of (b–d) Nb-doped microspheres. Secondary electrode imaging was used for b and d and backscattered imaging was used for a and c.

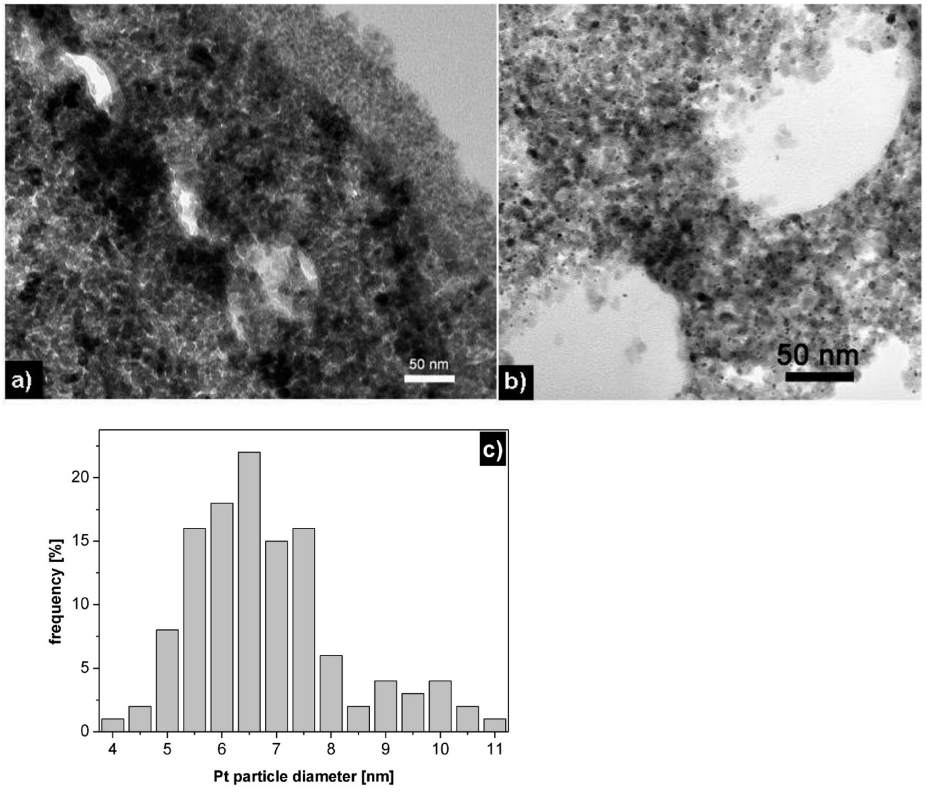

Figure 3. TEM micrographs of microtomed sections of (a) Nb-doped TiO_2 microspheres, (b) 20 wt %Pt/Nb-doped TiO_2 support. (c) Size distribution of Pt nanoparticles in 20 wt %Pt/Nb-doped TiO_2 samples.

demonstrates a good homogeneity with an average pore size of 4 nm. The interparticle porosity detected by this measurement is in agreement with the agglomeration of nanoparticles observed by TEM. The specific surface area calculated with the BET equation was 150 $m^2\ g^{-1}$ for 5 at % Nb-doped titania, and 120 $m^2\ g^{-1}$ for 10 at % Nb-doped titania. The results shown in the following paragraphs are for the material with the higher specific surface area, namely 5 at % Nb-doped TiO_2.

The core-level binding energies (BE) determined by XPS analysis for both undoped and doped TiO_2 powders are

dx.doi.org/10.1021/am300002j | ACS Appl. Mater. Interfaces 2012, 4, 1752–1759

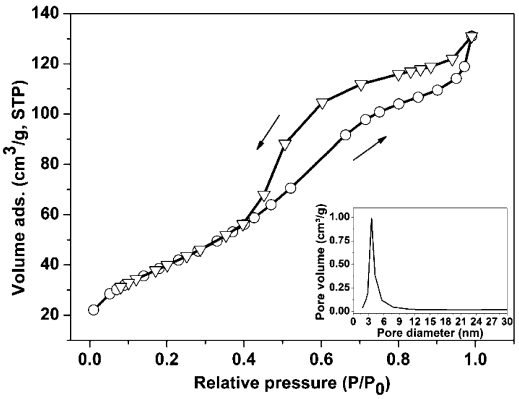

Figure 4. N_2 adsorption/desorption isotherms of the Nb-doped TiO_2 after calcination in air at 500 °C. The inset shows the pore size distribution of the Nb-doped TiO_2 powders.

summarized in Table 1. In the spectra of Ti $2p_{3/2}$ region, the peaks are centered at 458.9 and 459.2 eV for undoped and doped TiO_2, respectively (graphs are not shown). This indicates an oxidation state of Ti^{4+}. In agreement with the literature, the slightly higher BE value obtained for doped TiO_2 compared to that obtained for undoped TiO_2, can be explained by a change in the Fermi level due to the Nb doping.[16,23,58] For the Nb-doped TiO_2 sample, the Nb 3d structure which shows a doublet peak centered at 207.6 and 210.4 eV indicates the presence of Nb^{5+}. In all cases, the strong peak of BE for O 1s reported in the table corresponds to bulk oxygen bonded to titanium. Since neither detectable amounts of Ti^{2+} or Ti^{3+}, nor traces of Nb^{4+} were detected, it can be assumed that during doping with niobium, the charge compensation of Nb^{5+} is preferentially achieved by the creation of one vacancy per titanium site per four Nb atoms introduced. The occurrence of oxygen vacancies, electron holes or interstitials for titanium also has to be considered. These Nb-doped TiO_2 defects would then introduce electronic disorder, which would lead to higher electronic conductivity.[23,59] Indeed, the room temperature electronic conductivity increases from 1×10^{-8} S/cm for the nondoped titania microspheres to 1×10^{-4} S/cm for 5 at % Nb-doped TiO_2. All these characterizations confirm the effective doping of TiO_2 with niobium and the generation of mesoporous microspheres. This material was thus investigated as a catalyst support, by depositing Pt nanoparticles and studying the overall electrochemical properties.

Table 1. Binding Energies of the XPS Bands

	BE (eV)		
peaks	undoped TiO_2	5 at % Nb-doped TiO_2	20 wt % Pt/Nb-doped TiO_2
Ti $2p_{3/2}$	458.9	459.2	459
Ti $2p_{1/2}$	464.6	464.9	464.7
Nb $3d_{5/2}$		207.6	207.5
Nb $3d_{3/2}$		210.4	210.3
Pt $4f_{7/2}$			70.6
Pt $4f_{5/2}$			73.9
O 1s	530.1	530.4	530.3

Electrode Characterization. From the XRD pattern shown in Figure 1c, it was verified that the Pt coated doped TiO_2 was present in anatase form. The second contribution identified on this pattern is that of platinum Pt^0 (JCPDS 04–0802). Calculations using the Scherrer equation provided a dimension of the Pt particles in the 4–6 nm range. Observing the microtomed samples (and thus the cross sections of the microspheres) prepared for the 20 wt % Pt/Nb-doped TiO_2 sample, both SEM and TEM analysis at low magnification (not shown here), confirmed that the support nanostructure did not collapse during the microwave treatment. Figure 3b shows the TEM micrograph of a microtomed section (at high magnification) after the Pt deposition. The small Pt particles can be clearly distinguished and their size was estimated as 5–7 nm (Figure 3c), which is in good agreement with the domain size estimated from XRD. The dispersion was uniform and no aggregates of Pt were observed.

Figure 5 shows the core level spectra of Nb 3d, Ti 2p, and Pt 4f obtained from XPS analysis on the 20 wt %Pt/Nb-doped TiO_2 support, whereas the values of BE obtained are reported in Table 1. After the microwave assisted deposition of Pt, the Nb 3d structure shows a doublet peak centered at 207.5 and 210.3 eV, which still indicates the Nb^{5+} oxidation state. The shape of the signals excludes the presence of Nb^{4+}, which would be indicated by a signal separated by almost 2 eV from the Nb^{5+} peak. The doublet peak for Ti 2p demonstrates that only the Ti^{4+} state is present. The shape of the spectrum also excludes the presence of trace amounts of Ti^{2+} or Ti^{3+}. From the core-level spectrum in the platinum region, it can be clearly seen that only the Pt^0 state is present with a BE of 70.6 eV for Pt $4f_{7/2}$, in good agreement with the literature.[60–62] This confirms that this microwave method leads to direct reduced Pt and thus no further H_2 treatment was necessary.

Electrochemical Properties. To assess the electrochemical properties of the Nb-TiO_2 supported Pt, cyclic voltammetry measurements were carried out in 0.5 M H_2SO_4 at a scan rate of 100 mV s^{-1} over 1000 cycles. To evaluate its stability, the cyclic voltammograms (CV) after 100, 500, and 1000 cycles of the Nb-TiO_2 supported Pt sample were compared to the corresponding voltammograms of reference Pt/C (E-Tek), as shown in panels a and b Figure 6, respectively. The Pt loading on the RDE was 48 μg cm^{-2} (geometric area) in both cases.

Typical hydrogen adsorption/desorption peaks in the potential range of 0.05–0.35 V vs RHE and Pt oxide formation (>0.8 V) and reduction (0.5–1 V) were clearly observed for both supports. A distinct double-layer region with an almost constant current in the range of 0.35–0.65 V vs RHE was observed for the CV with Nb-TiO_2, indicating its resistance toward oxidation when subjected to high positive potentials. For the CV with carbon, a convoluted peak could be observed for the cathodic sweep at 0.6–0.75 V, which might be due to interactions with functional groups on the carbon surface and the reduction of platinum oxide.[33] For both samples, a decrease of the active Pt area was observed during continuous cycling, as indicated, for example, by the decrease of the hydrogen desorption peaks (0.05–0.35 V vs RHE) and of the platinum oxide reduction peaks (0.75–0.80 V). On the basis of the CV results, it was evident that the degradation over time was stronger for the reference Pt/C based sample relative to Nb-TiO_2. This was confirmed by calculating the electroactive Pt area after 100, 500, and 1000 cycles. For the Nb-TiO_2 supported catalyst, starting from an active Pt area of 30 m^2 g^{-1} (at 100 cycles), about 88 and 85% of the active Pt surface area remained after 500 and 1000 cycles, respectively. For the reference Pt/C supported catalyst, starting from an active Pt area of 36 m^2 g^{-1}, only 70 and 47% of the active Pt area remained after 500 and 1000 cycles, respectively. Even if the

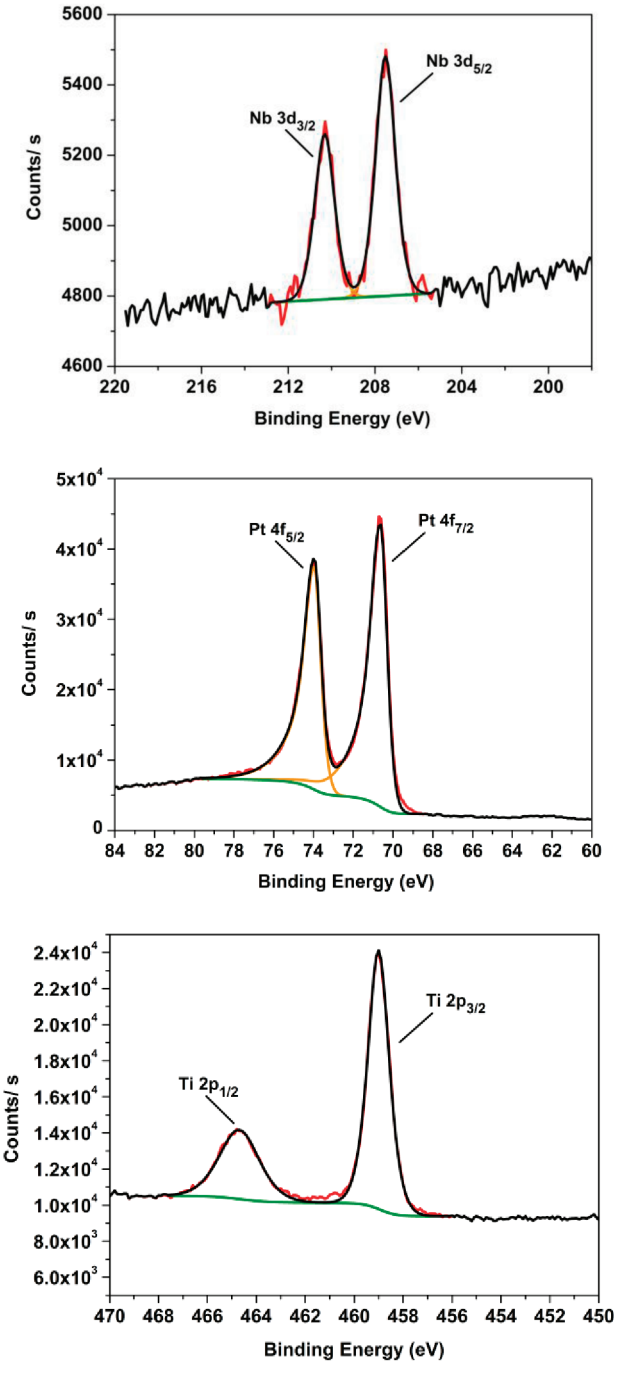

Figure 5. Core-level spectra of the elements analyzed by XPS measurements on 20 wt % Pt/Nb-doped TiO_2 support.

initial active Pt area was slightly lower, the Nb-doped titania supported catalyst demonstrated significantly higher stability, which can be explained both by strong Pt-TiO_2 interactions and better electro/chemical stability of the electroceramic support. Indeed, the resistance to electrochemical corrosion of the ceramic support over that of carbon is considered a key factor to the observed relative stability of the electrochemically active surface area of Pt on Nb-doped titania.

Figure 7 shows the linear sweep voltammograms obtained for Pt supported on Nb-TiO_2 and for Pt supported on carbon. The solid lines show the ORR measurement recorded for the freshly prepared catalyst, i.e., before the voltammetric stability test, while the dashed lines show the ORR recorded for the "aged"

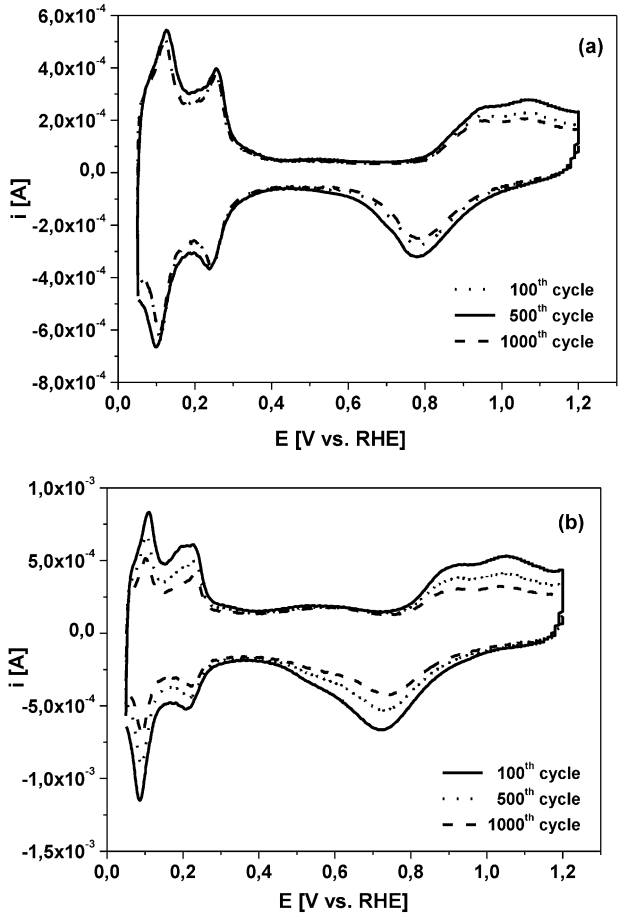

Figure 6. Cyclic voltammograms obtained after 100, 500, and 1000 cycles for (a) Pt/5 at % Nb-TiO_2 and (b) Pt/C.

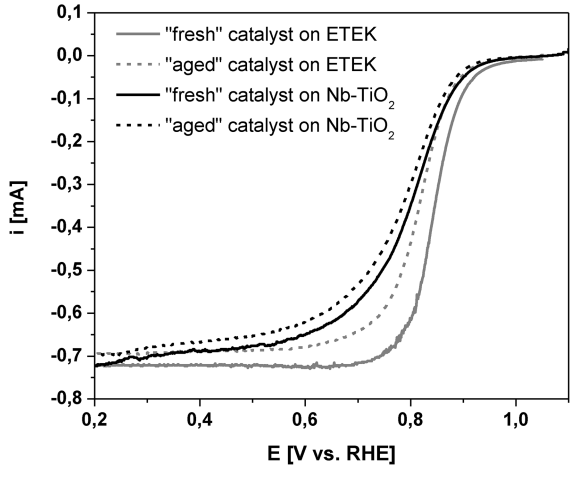

Figure 7. Oxygen reduction experiments in oxygen saturated electrolyte, at a rotation rate of 900 rpm. Black lines are for the Nb-TiO_2-supported Pt, and gray lines are for the carbon-supported Pt.

catalyst, i.e., after 1000 potential cycles, as explained in the Experimental Section. In both cases, the ORR proceeded under mixed kinetic-diffusion control in the potential region between 0.95 and 0.6 V, followed by a region with a diffusion limited current. The onset potential was fairly high. Comparing both samples, the reference Pt/C demonstrated the better performance, which was expected due to its higher specific Pt surface area and the higher conductivity of the support. However, it

dx.doi.org/10.1021/am300002j | ACS Appl. Mater. Interfaces 2012, 4, 1752−1759

was also observed that the degradation of the oxygen reduction activity was more pronounced in the case of Pt/C compared to Pt/Nb-TiO_2. This was confirmed by the calculation of the mass activity at 0.9 V vs RHE. In the case of the Pt/Nb-TiO_2 sample, the mass activity decreased from 5.3 to 3.6 A g_{Pt}^{-1} (fresh and aged catalyst, respectively), thus showing a deterioration of the ORR activity of 32%. In the case of the reference Pt/C sample, the mass activities were 9.2 and 4.7 A g_{Pt}^{-1} for the fresh and aged catalyst state, respectively, thus showing a deterioration of the ORR activity of 49%. This loss in ORR activity can be explained by the instability of the carbon support under oxidizing conditions.

CONCLUSIONS

The use of an acid-functionalized ionomer as a reaction and templating medium with appropriate inorganic precursors in solution in a high dielectric constant solvent provides a novel and simple synthesis for the formation of Nb-doped anatase microspheres having an internal porosity gradient. Preliminary electrochemical analysis indicated that Nb-doped TiO_2 is a promising support for Pt nanoparticles deposited using a microwave assisted method. The high stability of the electrochemical surface area during continuous cycling relative to that obtained using a conventional carbon support is encouraging for further application of these materials in PEM fuel cell electrodes, in particular at operation temperatures higher than those of conventional PEMFC. Further studies varying the Nb content and support morphology are in progress.

AUTHOR INFORMATION

Corresponding Author

*E-mail: Deborah.Jones@univ-montp2.fr.

Notes

The authors declare no competing financial interest.

ACKNOWLEDGMENTS

This work was funded through the collaborative Programme in Nanosciences between the Centre National de la Recherche Scientifique (CNRS) and the National Research Council of Canada (CNRC). Dr. Laure Chevallier thanks the CNRS for a postdoctoral fellowship.

REFERENCES

(1) Zhang, J.; Xie, Z.; Zhang, J.; Tang, Y.; Song, C.; Navessin, T.; Shi, Z.; Song, D.; Wang, H.; Wilkinson, D. P.; Liu, Z.-S.; Holdcroft, S. *J. Power Sources* **2006**, *160*, 872.
(2) Shao, Y.; Yin, G.; Wang, Z.; Gao, Y. *J. Power Sources* **2007**, *167*, 235.
(3) Rozière, J.; Jones, D. J. *Annu. Rev. Mater. Res.* **2003**, *33*, 503.
(4) Mocoteguy, Ph.; Ludwig, B.; Scholta, J.; Nedellec, Y.; Jones, D. J.; Rozière, J. *Fuel Cells* **2010**, *10*, 299.
(5) Masao, A.; Noda, S.; Takasaki, F.; Ito, K.; Sasaki, K. *Electrochem. Solid-State Lett.* **2009**, *12*, B119.
(6) Antolini, E. *Appl. Catal. B* **2009**, *88*, 1.
(7) Shao, Y.; Liu, J.; Wang, Y.; Lin, Y. *J. Mater. Chem.* **2009**, *19*, 46.
(8) Schmittinger, W.; Vahidi, A. *J. Power Sources* **2008**, *180*, 1.
(9) Shao, Y.; Yin, G.; Gao, Y. *J. Power Sources* **2007**, *171*, 558.
(10) Antolini, E.; Gonzalez, E. R. *Solid State Ionics* **2009**, *180*, 746.
(11) White, J. H.; Sammells, A. F. *J. Electrochem. Soc.* **1993**, *140*, 2167.
(12) Wesselmark, M.; Wickman, B.; Lagergren, C.; Lindbergh, G. *Electrochim. Acta* **2010**, *55*, 7590.
(13) Sasaki, K.; Zhang, L.; Adzic, R. R. *Phys. Chem. Chem. Phys.* **2008**, *10*, 159.
(14) Tauster, S. J.; Fung, S. C.; Baker, R. T. K.; Horsley, J. A. *Science* **1981**, *211*, 1121.
(15) Haas, O. E.; Briskeby, S. T.; Kongstein, O. E.; Tsypkin, M.; Tunold, R.; Boressen, B. T. *J. New Maer. Electrochem. Syst.* **2008**, *11*, 9.
(16) Moreno, B.; Chinarro, E.; Fierro, J. L. G.; Jurado, J. R. *J. Power Sources* **2007**, *169*, 98.
(17) Siracusano, S.; Baglio, V.; D'Urso, C.; Antonucci, V.; Aricò, A. S. *Electrochim. Acta* **2009**, *54*, 6292.
(18) Chen, G.; Rare, S. R.; Mallouk, T. E. *J. Electrochem. Soc.* **2002**, *149*, A1092.
(19) Ioroi, T.; Siroma, Z.; Fujiwara, N.; Yamazaki, S.-I.; Yasuda, K. *Electrochem. Commun.* **2005**, *7*, 183.
(20) Garcia, B. L.; Fuentes, R.; Weidner, J. W. *Electrochem. Solid-State Lett.* **2007**, *10*, B108.
(21) Park, K. W.; Seol, K. S. *Electrochem. Commun.* **2007**, *9*, 2256.
(22) Chhina, H.; Susac, D.; Campbell, S.; Kesler, O. *Electrochem. Solid-State Lett.* **2009**, *12*, B97.
(23) Ruiz, A. M.; Dezanneau, G.; Arbiol, J.; Cornet, A.; Morante, J. R. *Chem. Mater.* **2004**, *16*, 862.
(24) Arbiol, J.; Cerda, J.; Dezanneau, G.; Cirera, A.; Peiro, F.; Cornet, A.; Morante, J. R. *J. Appl. Phys.* **2002**, *92*, 853.
(25) Sato, Y.; Akizuki, H.; Kamiyama, T.; Shigesato, Y. *Thin Solid Films* **2008**, *516*, 5758.
(26) Elezović, N. R.; Babić, B. M.; Gajić-Krstajić, L.; Radmilović, V.; Krstajić, N. V.; Vračar, L. J. *J. Power Sources* **2010**, *195*, 3961.
(27) Antonelli, D. M.; Ying, J. Y. *Angew. Chem., Int. Ed.* **1995**, *34*, 2014.
(28) On, D. T. *Langmuir* **1999**, *15*, 8561.
(29) Shibata, H.; Mihara, H.; Mukai, T.; Ogura, T.; Kohno, H.; Ohkubo, T.; Sakai, H.; Abe, M. *Chem. Mater.* **2006**, *18*, 2256.
(30) Baglio, V.; Di Blasi, A.; Aricò, A. S.; Antonucci, V.; Antonucci, P. L.; Trakanprapai, C.; Esposito, V.; Licoccia, S.; Traversa, E. *J. Electrochem. Soc.* **2005**, *152*, A1373.
(31) Yoshitake, H.; Sugihara, T.; Tatsumi, T. *Chem. Mater.* **2002**, *14*, 1023.
(32) Antonelli, D. M. *Microporous Mesoporous Mater.* **1999**, *30*, 315.
(33) Yang, P.; Zhao, D.; Margolese, D. I.; Chmelka, B. F.; Stucky, G. D. *Chem. Mater.* **1999**, *11*, 2813.
(34) Zheng, J.-Y.; Pang, J.-B.; Qiu, K.-Y.; Wei, Y. *J. Mater. Chem.* **2001**, *11*, 3367.
(35) Soler-Illia, G. J. d. A. A.; Crepaldi, E. L.; Grosso, D.; Sanchez, C. *Curr. Opin. Colloid Interface Sci.* **2003**, *8*, 109.
(36) Ye, M.-M.; Chen, Z.-L.; Wang, W.-S.; Zhen, L.; Shen, J.-M. *Chem. Lett.* **2008**, *37*, 938.
(37) Bao, S.-J.; Bao, Q.-L.; Li, C.-M.; Zhi-Li, D. *Electrochem. Commun.* **2007**, *9*, 1233.
(38) Madhugiri, S.; Sun, B.; Smirniotis, P. G.; Ferraris, J. P.; Balkus, K. J. *Microporous Mesoporous Mater.* **2004**, *69*, 77.
(39) Wang, M.; Guo, D.-J.; Li, H.-L. *J. Solid State Chem.* **2005**, *178*, 1996.
(40) Cavaliere, S.; Subianto, S.; Chevallier, L.; Jones, D. J.; Rozière, J. *Chem. Commun.* **2011**, *47*, 6834.
(41) Bauer, A.; Lee, K.; Song, C.; Xie, Y.; Zhang, J.; Hui, R. *J. Power Sources* **2010**, *195*, 3105.
(42) Shanmugam, S.; Gedanken, A. *J. Phys. Chem. C* **2009**, *113*, 18707.
(43) Bauer, A.; Song, C.; Ignaszak, A.; Hui, R.; Zhang, J.; Chevallier, L.; Jones, D.; Rozière, J. *Electrochim. Acta* **2010**, *55*, 8365.
(44) Cavaliere, S.; Subianto, S.; Savych, I.; Jones, D. J.; Rozière, J. *Energy Environ. Sci.* **2011**, *4*, 4761−4785.
(45) von Kraemer, S.; Wikander, K.; Lindbergh, G.; Lundblad, A.; Palmqvist, A. E. C. *J. Power Sources* **2008**, *180*, 185.
(46) Huang, S.-Y.; Ganesan, P.; Park, S.; Popov, B. N. *J. Am. Chem. Soc.* **2009**, *131*, 13898.
(47) Song, Y.-Y.; Gao, Z.-D.; Schmuki, P. *Electrochem. Commun.* **2011**, *13*, 290.
(48) Tamaki, R.; Chujo, Y. *Chem. Mater.* **1999**, *11*, 1719.

(49) Jones, D. J.; Rozière, J. *Adv. Polym. Sci.* **2008**, *215*, 219.
(50) Bauer, B.; Jones, D. J.; Rozière, J.; Tchicaya, L.; Alberti, G.; Casciola, M.; Massinelli, L.; Peraio, A.; Besse, S.; Ramunni, E. *J. New Mater. Electrochem. Syst.* **2000**, *3*, 93.
(51) Traversa, E.; Di Vona, M. L.; Licoccia, S.; Sacerdoti, M.; Carotta, M. C.; Crema, L.; Martinelli, G. *J. Sol−Gel Sci. Technol.* **2001**, *22*, 167.
(52) Li, X.; Chen, W.-X.; Zhao, J.; Xing, W.; Xu, Z.-D. *Carbon* **2005**, *43*, 2168.
(53) Brunauer, S.; Emmet, P. H.; Teller, E. *J. Am. Chem. Soc.* **1938**, *60*, 309.
(54) Shirley, D. A. *Phys. Rev. B* **1972**, *5*, 4709.
(55) Scofield, J. H. *J. Electron Spectrosc. Relat. Phenom.* **1976**, *8*, 129.
(56) Nart, F. C.; Vielstich, W. *Handbook of Fuel Cells: Fundamentals, Technology and Application*; J. Wiley and Sons: New York, 2003; Vol. 2.
(57) Xu, T.; Zhang, H.; Zhong, H.; Ma, Y.; Jin, H.; Zhang, Y. *J. Power Sources* **2010**, *195*, 8075.
(58) Morris, D.; Dou, Y.; Rebane, J.; Mitchell, C. E. J.; Egdell, R. G.; Law, D. S. L.; Vittadini, A.; Casarin, M. *Phys. Rev. B* **2000**, *61*, 13445.
(59) Eror, N. G. *J. Solid State Chem.* **1981**, *38*, 281.
(60) Kim, K. S.; Winograd, N.; Davis, R. E. *J. Am. Chem. Soc.* **1971**, *93*, 6296.
(61) Spichiger-Ulmann, M.; Monnier, A.; Koudelka, M.; Augustynski, J. *Spectroscopic and Electrochemical Study of the State of Pt in Pt-TiO_2/ Catalysts*; American Chemical Society,: Washington, D.C., 1986.
(62) Raynal, F.; Etcheberry, A.; Cavaliere, S.; Noël, V.; Perez, H. *Appl. Surf. Sci.* **2006**, *252*, 2422.